Chemical Geology 464 (2017) 76–83

Contents lists available at ScienceDirect

Chemical Geology

journal homepage: www.elsevier.com/locate/chemgeo

Sorption of Se(IV) and Se(VI) to coal fly ash/cement composite: Effect of Ca^{2+} and high ionic strength

Weiling Sun [a,b], Jay E. Renew [b], Wenlong Zhang [b], Yuanzhi Tang [c], Ching-Hua Huang [b,*]

[a] College of Environmental Sciences and Engineering, Peking University, The Key Laboratory of Water and Sediment Sciences, Ministry of Education, Beijing 100871, China
[b] School of Civil and Environmental Engineering, Georgia Institute of Technology, Atlanta, GA 30332, United States
[c] School of Earth and Atmospheric Sciences, Georgia Institute of Technology, Atlanta, GA 30332, United States

ARTICLE INFO

Article history:
Received 21 October 2016
Received in revised form 20 December 2016
Accepted 28 December 2016
Available online 30 December 2016

Keywords:
Selenate
Selenite
FGD wastewater
Coal fly ash
Sorption mechanism
Se immobilization

ABSTRACT

The sorption behavior and mechanisms of Se from wastewater with high salinity are unclear, a scenario that can be encountered in the flue-gas-desulfurization (FGD) blowdown at coal-fired power plants. In this study, we investigated the uptake behavior and mechanisms of Se(IV) and Se(VI) by a coal fly ash/cement composite at high ionic strengths (IS) of up to 3.0 M NaCl or $CaCl_2$ using batch sorption experiments, Fourier-transform infrared spectroscopy, X-ray photoelectron spectroscopy, X-ray diffraction, and X-ray absorption spectroscopy. NaCl, regardless of IS, only caused slight changes in Se(IV) and Se(VI) uptake. Presence of $CaCl_2$ significantly enhanced Se(IV) uptake, but had minor effect at low IS (≤0.3 M) and no effect at high IS (>0.3 M) on Se(VI) uptake. Both Se(IV) and Se(VI) mainly formed outer-sphere surface complexes in the presence of NaCl. The enhanced Se(IV) uptake by $CaCl_2$ is likely due to the formation of Ca-SeO_3 precipitate(s). Outer-sphere complexation is the main mechanism for Se(VI) sorption in the presence of $CaCl_2$, with additional formation of minor amounts of inner-sphere complex at IS > 0.3 M. The results added new mechanistic insights for Se removal from industrial wastewaters with high salinity and will be useful for immobilization of Se in the co-management of FGD blowdown and coal fly ash wastes.

1. Introduction

Selenium (Se) is an essential micronutrient for plants and humans, but is toxic if taken in excess (Fordyce, 2007). Se can accumulate in aquatic organisms through food chains and affect the health and reproduction of trophic-end members such as fish and aquatic birds (Lemly, 1993; Luoma and Presser, 2009; Ruhl et al., 2012). The USEPA has set the maximum contaminant level for total Se in drinking water at 50 μg/L and the ambient water quality criterion for Se in freshwater at 1.5–3.1 μg/L (USEPA, 2003; http://www.epa.gov/wqc/aquatic-life-criterion-selenium). The World Health Organization (WHO) has recommended a drinking water limit of 40 μg/L for Se (WHO, 2011). In natural environment, Se can exist in four valence states, elemental Se (Se(0)), metal selenides or organic selenides (Se(-II)), and oxyanions selenite (Se(IV), SeO_3^{2-}) and selenate (Se(VI), SeO_4^{2-}) (Chappell et al., 2014). Se(IV) and Se(VI) are the primary forms in fresh water environments (Conde and Sanz Alaejos, 1997; Lai et al., 2014), while Se(0) and Se(-II) (as organic selenides) are often the dominant species in freshwater and estuarine sediments (Meseck and Cutter, 2012).

The presence of Se(IV)/(VI) in wastewater is of particular concern because of their toxicity to humans and animals at high exposures (Ruhl et al., 2010; Schwartz et al., 2016). At coal-fired power plants, flue-gas-desulfurization (FGD) systems are employed to control SO_x air pollution and 69% of coal-fired capacity will be wet scrubbed by 2025 (USEPA, 2009). FGD wastewaters contain significant concentrations of metal(loid)s (e.g. Se) and total dissolved solids (TDS) (up to 50,000 mg/L, predominantly Ca^{2+} and Cl^- salts) (Huang et al., 2012), which will negatively impact the water quality of receiving waters (Ruhl et al., 2012). There are forced-oxidation, natural oxidation, and inhibited oxidation types of FGD systems, with the forced oxidation systems being the main type to be constructed (EPRI, 2008; USEPA, 2009). In a forced oxidation system, air is pumped through FGD to oxidize SO_3^{2-} to SO_4^{2-}, which precipitates as $CaSO_4 \cdot 2H_2O$ (gypsum), a salable product for wallboard or soil amendment (EPRI, 2008). Metal(loid)s including Se can also be oxidized in the forced oxidation systems.

The coupling of brine concentration with solidification/stabilization (S/S) processes for FGD wastewater treatment is an emerging technology in the coal-fired power industry. S/S typically includes mixing of wastes with Portland cement (PC), PC/coal fly ash (CFA), CaO/CFA, or $Ca(OH)_2$/CFA (Batchelor, 2006). Strong interest in this emerging "zero liquid discharge (ZLD)" approach has led to pilot-scale testing and potential full-scale implementation. Our recent studies have demonstrated that S/S of FGD brine with CFA and PC was effective in retaining Se in the produced composite, although the efficiency varied for Se(IV) and Se(VI) under different conditions (Huang et al., 2016; Renew et

* Corresponding author.
E-mail address: ching-hua.huang@ce.gatech.edu (C.-H. Huang).

http://dx.doi.org/10.1016/j.chemgeo.2016.12.041
0009-2541/

al., 2016). Thus, understanding the speciation and immobilization mechanism(s) of Se(IV)/(VI) by the CFA/PC composite is critical for assessing the long-term fate and mobility of the immobilized Se.

The mechanisms for Se immobilization in the S/S system are likely surface adsorption, complexation, ion exchange, and/or precipitation (Baur and Johnson, 2003; Bonhoure et al., 2006; Johnson et al., 2000). One challenge for obtaining mechanistic information in this system is the presence of high ionic strength (IS) from the brine. Although adsorption is commonly employed for removing Se from aqueous systems, most previous studies were conducted under low IS. For example, the adsorption of Se(IV)/(VI) by various metal oxides (Elzinga et al., 2009; Jordan et al., 2011, 2013a, 2013b, 2014; Peak and Sparks, 2002; Chan et al., 2009; Sun et al., 2015) has been widely studied. Depending on mineral type, Se(IV)/(VI) can form outer- and/or inner-sphere surface complexes (Jordan et al., 2011, 2013a, 2013b, 2014; Manceau and Charlet, 1994; Peak, 2006; Peak and Sparks, 2002; Sun et al., 2015; Wijnja and Schulthess, 2000). Se(IV) was found to adsorb much more strongly than Se(VI) to goethite, due to the formation of strong inner-sphere complex of Se(IV) versus the weak outer-sphere complex of Se(VI) (Balistrieri and Chao, 1987; Hayes et al., 1987). However, despite the potential importance to FGD wastewater treatment, the removal mechanisms of Se under high salinity condition were overall much less investigated.

Another challenge for studying Se removal in the S/S system is that all the solid phases involved in the treatment process (CFA, PC, and final composite) have complex structure and compositions. The distribution coefficients (K_d) for oxyanion uptake by cement are typically low because oxyanion sorption typically decreases with increasing pH (Ochs et al., 2002). However, Keller (2002) found high uptake of Se(IV) to the main mineral components of cement (ettringite, monosulfate, and calcium silicate hydrate), while Se(VI) sorption to monosulfate was stronger than to the other two minerals. CFA and PC contain various metal oxides such as SiO_2, Al_2O_3, Fe_2O_3, and CaO (Ochs et al., 2002; Renew et al., 2016), each may interact differently with Se(IV)/(VI). Therefore, the retention mechanisms of Se(IV)/(VI) by the composites in the treatment process are far more complex than that by a single mineral.

The objective of this study was to investigate the uptake mechanism(s) of Se(IV)/(VI) to the CFA/PC composite that was formed from the S/S treatment of FGD brines using a model system with controlled experimental conditions. The uptake of Se(IV)/(VI) by the CFA/PC composite was investigated in a simulated brine with two types of background electrolytes (NaCl and $CaCl_2$), IS of 0.03–3.0 M, and varied pH. In addition to batch sorption experiments, a suite of complementary techniques was applied, including Fourier-transform infrared (FT-IR) spectroscopy, X-ray photoelectron spectroscopy (XPS), X-ray diffraction (XRD), and X-ray absorption spectroscopy (XAS). This is among the first detailed study to investigate Se(IV) and Se(VI) immobilization by the fly ash/cement composite under high IS conditions.

2. Materials and methods

All experiments were performed in replicates. Details of experimental methods and sample information are reported in Supplementary data (Text S1 and Table S1).

2.1. Preparation of CFA/PC composite

The CFA from bituminous coal was obtained from a coal-fired power plant in the southeastern United States. The PC was a Type I/II cement purchased from the Home Depot. The CFA/PC composite was prepared by mixing CFA (60 wt%), PC (10 wt%), and ultrapure water (30 wt%) for 20 min and allowed to cure for 13 d in a humid environment according to our previous study (Renew et al., 2016). The cured solid was ground and sieved (170 mesh, 88 μm).

2.2. Se(IV)/(VI) sorption experiments

Batch sorption experiments of Se to the CFA/PC composite were conducted under varied background electrolyte type and concentration, pH, and Se concentration (Table S1). Experiments were conducted in acid-washed plastic bottles by adding 1.0 g of composite to 50 mL solutions (i.e., 20 g/L) containing NaCl or $CaCl_2$ at IS of 0.03, 0.3, 1.5, or 3.0 M. The NaCl or $CaCl_2$ solutions served as analogs to the FGD brine with a wide range of salinity and composition. Concentrated Se(IV) (as Na_2SeO_3) or Se(VI) (as Na_2SeO_4) stock solutions were added to the mixed suspension to achieve initial Se concentrations of 0.01–1.5 mM. The reaction bottles were shaken at 250 rpm and 25 ± 1 °C for 24 h to allow equilibrium. Sorption isotherms were conducted without pH adjustment, and the final pH was around 11.0 ± 0.7. At the end of experiment, aliquots of the reaction suspension were filtered (0.45 μm cellulose acetate membranes) and acidified by HNO_3 for Se concentration analysis by inductively coupled plasma – optical emission spectroscopy (ICP-OES) (Text S1). Se adsorption to the bottles and filter membranes were confirmed negligible. Another set of experiments were also conducted to investigate the influence of pH (2–12, adjusted by HCl or NaOH) on Se uptake, with 3.0 M IS (NaCl or $CaCl_2$) and the initial Se(IV) or Se(VI) concentration of 1.0 mM. The samples were reacted for 24 h, and the equilibrium pH was measured.

2.3. Sample characterization

The solid samples from the sorption experiments in which Se(IV) or Se(VI) was sorbed to the CFA/PC composite in NaCl or $CaCl_2$ media are labeled as "sorbed Se(IV)-Na", "sorbed Se(VI)-Na", "sorbed Se(IV)-Ca" and "sorbed Se(VI)-Ca". Depending on the sensitivity of characterization techniques, appropriate concentrations of Se(IV)/(VI) or IS were employed (detailed in Text S1 and Table S1). Additionally, a precipitation experiment was conducted by combining equal volumes of 1.0 M Na_2SeO_3 and 1.0 M $CaCl_2$ to produce a Ca-Se(IV) precipitate (termed "Ca-Se(IV) precipitate") (Text S1). The unreacted CFA, PC, and CFA/PC composite, as well as powders of Na_2SeO_3, Na_2SeO_4 and $CaSeO_3$ reagents were also characterized. The samples were characterized by zeta potential, attenuated total reflectance (ATR)-FT-IR, XRD, XPS and XAS (Details in Text S1).

3. Results and discussion

3.1. XRD characterization of solids before sorption

Both CFA and composite samples contained a large amount of amorphous phase(s), as indicated by the broad hump at 15–45° 2θ of their XRD patterns (Fig. S1a and c), and were consistent with previous studies (Lo et al., 2000). The main crystalline phases of CFA were quartz and mullite (Fig. S1a and Table S2). The XRD pattern of PC showed the peaks of dicalcium silicates, tricalcium silicates, tricalcium aluminate, and calcium aluminoferrite (Fig. S1b and Table S2), consistent with the typical composition of PC. The detected crystalline phases for the composite (Fig. S1c) matched well with the XRD peaks of CFA and PC. A small amount of a new phase portlandite, $Ca(OH)_2$, was also found in the composite sample (Table S2). The results were consistent with our previous study, which showed that the main chemical compositions were SiO_2 (54.3%), Al_2O_3 (25.2%) and Fe_2O_3 (11.9%) for CFA, CaO (63.8%) and SiO_2 (21.7%) for PC, and SiO_2 (40.1%), CaO (26.4%) and Al_2O_3 (19.7%) for the CFA/PC composite (Renew et al., 2016).

3.2. Sorption isotherms

The CFA/PC composite showed high adsorption capacities for both Se(IV) and Se(VI) (Fig. 1). In NaCl medium, the sorption of Se(IV) and Se(VI) increased only slightly with increasing IS from 0.03 to 3.0 M, with the overall sorption amounts of Se(IV) slightly greater than those

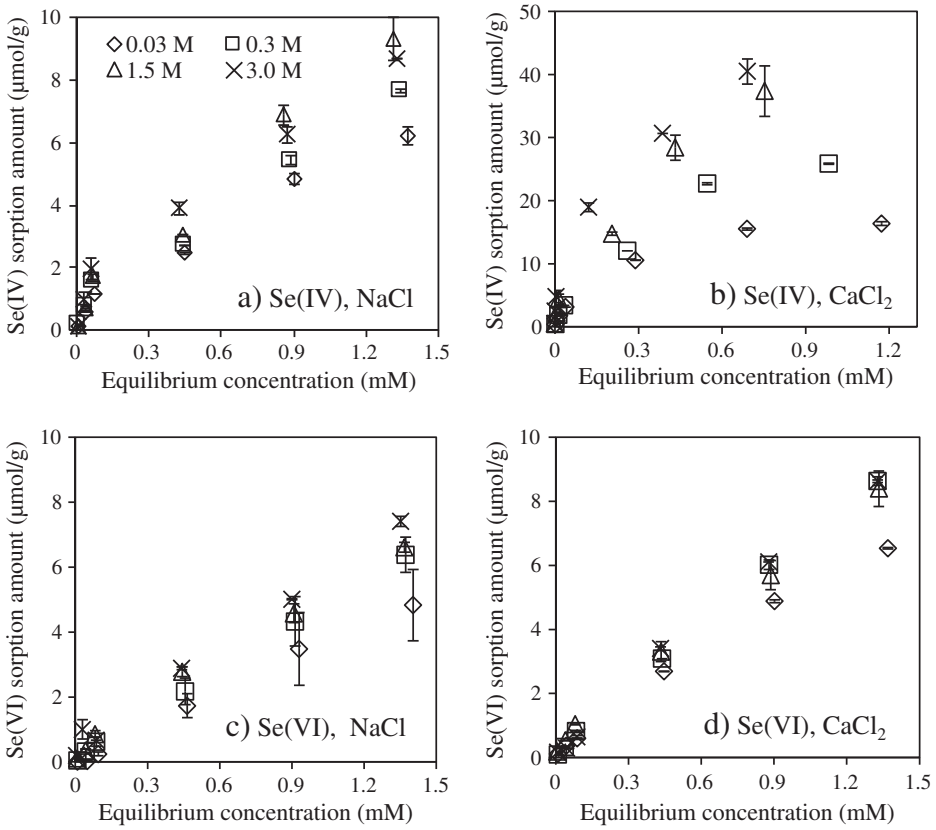

Fig. 1. Sorption isotherms of (a, b) Se(IV) and (c, d) Se(VI) by composite at different ionic strengths (0.03 to 3.0 M) of NaCl or $CaCl_2$. pH was not adjusted for isotherm experiments and the final pH values are ~11.0 ± 0.7.

of Se(VI) at all IS levels (Fig. 1a,c). In $CaCl_2$ medium, the sorption amount of Se(VI) slightly increased when the IS changed from 0.03 to 0.3 M (Fig. 1d), whereas no IS effect was observed at higher IS of 0.3–3.0 M. However, the sorption amount of Se(IV) was enhanced significantly with increasing IS of $CaCl_2$ from 0.03 to 3.0 M (Fig. 1b). Both Langmuir and Freundlich isotherm models were used to fit the sorption data, and the results are discussed in Text S2.

Based on the thermodynamic data for metal selenites (Elrashidi et al., 1987; Essington, 1988; Sharmasarkar et al., 1996), it was possible that the formation of Ca-Se(IV) complex(es) and/or precipitation of Ca-Se(IV) minerals occurred at high $CaCl_2$ concentrations, resulting in high uptake of Se(IV) by the composite. Indeed, Se(IV) was previously shown to form strong complex(es) and/or precipitates with divalent metal cations during sorption processes. Boyle-Wight et al. (2002a, 2002b) observed that Se(IV) enhanced Co(II) sorption to γ-Al_2O_3 due to the formation of Co(II)-Se(IV) complexes and/or precipitates, whereas Se(VI) did not affect Co(II) sorption to γ-Al_2O_3. It was also suggested that Mn(II)-Se(IV) precipitates may form during Se(IV) sorption to hydrous Mn oxides (Foster et al., 2003). Ochs et al. (2002) and Baur and Johnson (2003) have also suggested the potential formation of calcium selenite solids at higher initial Se(IV) concentrations during its uptake by cement.

3.3. Effect of pH

The effect of pH on Se(VI) and Se(IV) uptake by the composite was shown in Fig. 2. In NaCl medium, Se(IV) sorption decreased with increasing pH, from ~100% at pH 2.5 to ~10% at pH 11.5. In contrast, in $CaCl_2$ medium, Se(IV) sorption decreased with increasing pH from 2.5 to 9.5 and was maintained at ~40% between pH 9.5–11.5 (Fig. 2a). The

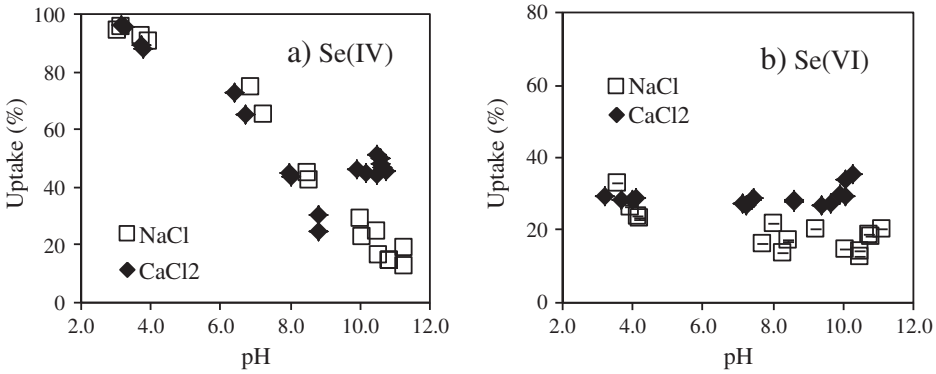

Fig. 2. Effect of pH on (a) Se(IV) and (b) Se(VI) uptake by the composite in the presence of 3.0 M of NaCl or $CaCl_2$.

increased Se(IV) sorption at high pH in $CaCl_2$ background electrolyte suggested the possible formation of Ca(II)-Se(IV) precipitation, which was consistent with the other results presented above. For Se(VI), a slight decrease of uptake was observed at pH 7.5–11.5 in NaCl medium. In $CaCl_2$ medium, uptake stayed constant at pH 2.5–9.5 and increased slightly with increasing pH at 9.5–11.5 (Fig. 2b). The reasons for the pH effect were further discussed in Text S3.

3.4. ATR-FT-IR analysis of Se(IV) sorption samples

ATR-FT-IR analysis (Fig. S3a) showed that the characteristic bands of Se(IV) aqueous solution varied with pH (Text S4) due to the change of Se(IV) speciation at various pHs (Text S5 and Fig. S4a) (Kretzschmar et al., 2015; Nakamoto, 2002; Su and Suarez, 2000). The band at 874 cm^{-1} of the composite sample after Se(IV) sorption in NaCl medium (Fig. 3a) was attributed to sorbed Se(IV), because this band was not observed in the spectra of uncreated CFA and CFA/PC composite samples (Fig. S3c and d). Se could form outer- and/or inner-sphere complexes with the composite. Generally, the formation of outer-sphere complexes only induces slight shifts of FT-IR peaks, whereas the formation of inner-sphere complexes will result in great shifts or splitting of bands (Ahrland, 1972; Jordan et al., 2013b; Nakamoto, 2009). However, monodentate and bidentate Se inner-sphere complexes are not distinguishable using FT-IR (Fowless and Stranks, 1977). Compared to the spectra of Se(IV) solution (Fig. S3a), the slight shifting of the 867 cm^{-1} band to higher wavenumber (around 874 cm^{-1}) (Fig. 3a) suggested the formation of outer-sphere complexes between Se(IV) and the composite.

For composite that adsorbed Se(IV) in $CaCl_2$ medium (Fig. 3c), multiple bands were observed and ascribed to sorbed Se(IV). Moreover, these bands altered with changing Ca(II) concentration. Five main bands (875, 840, 776, 746, and 700 cm^{-1}) were observed at lower Ca(II) concentrations (0.03 and 0.3 M), whereas four bands (875, 824, 746, and 726 cm^{-1}) were observed at the highest Ca(II) concentration (3.0 M). The sample at 1.5 M IS had intermediate characteristics and exhibited almost all the bands present at both lower and higher IS. Chubar (2014) observed several peaks at 760–768 cm^{-1} and 841–843 cm^{-1} after Se(IV) sorption on Mg-Al-CO_3 layered double hydroxide. Similar to that in NaCl medium (Fig. 3a), the band at 875 cm^{-1} resulted from the slight shifting of the 867 cm^{-1} band was present at all IS levels,

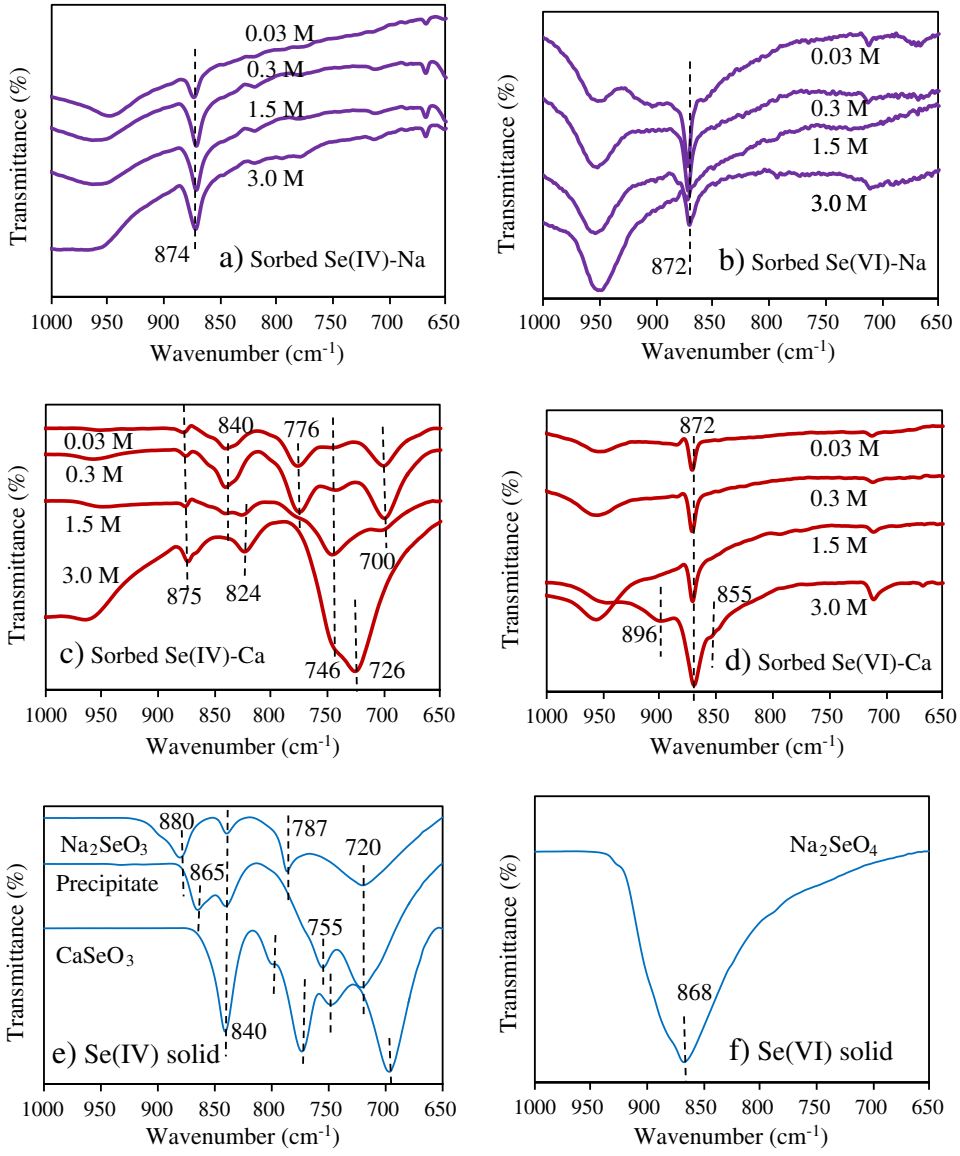

Fig. 3. ATR-FT-IR spectra of (a–d) composites after Se (IV)/(VI) sorption in NaCl or $CaCl_2$ background electrolyte, (e) pure Na_2SeO_3, pure $CaSeO_3$, Ca-Se(IV) precipitate formed in $CaCl_2$ + Na_2SeO_3 solution, and (f) pure Na_2SeO_4.

which indicated the formation of outer-sphere complex between Se(IV) and composite. The other bands were likely attributable to the formation of Ca-SeO_3 precipitate(s) or complex(es).

Indeed, reference compounds Na_2SeO_3, $CaSeO_3$, and Ca-Se(VI) precipitate (Fig. 3e) all had characteristics similar to the sorption samples. The solid Na_2SeO_3 had four bands at 880, 840, 787, and 720 cm^{-1}. $CaSeO_3$ had five bands at 840, 795, 774, 748, and 697 cm^{-1}, whereas the Ca-Se(IV) precipitate had four strong bands at 865, 840, 755, and 720 cm^{-1} (Fig. 3e). Compared with Na_2SeO_3, the bands of $CaSeO_3$ and Ca-Se(IV) precipitate moved toward lower wavenumbers due to the stronger bonding of Ca^{2+} with Se(IV) than that of Na^+ (Nakamoto, 2009). The five bands of $CaSeO_3$ were similar to those found for sorbed Se(IV)-Ca at 0.03 and 0.3 M IS (Fig. 3c), suggesting that precipitate with a structure similar to $CaSeO_3$ may dominate during Se(IV) sorption at lower Ca(II) concentration. The four bands of Ca-Se(IV) precipitate were different from those for sorbed Se(IV)-Ca at 3.0 M IS (Fig. 3c). This difference may indicate a new uptake mechanism occurring at this higher IS, possibly the formation of Ca(II)-Se(IV) precipitates with varied hydration states and/or the participation of carbonate or hydroxyl groups, or Ca-selenite-composite ternary surface complex(es). Previous studies on Co(II) sorption to γ-Al_2O_3 in the presence of Se(IV) suggested the formation of Co(II)-Al(III)-layered double hydroxides, mixed metal-selenite-hydrates, or a ternary complex at elevated Se(IV):Co(II) surface coverage ratios (Boyle-Wight et al., 2002a, 2002b).

3.5. ATR-FT-IR analysis of Se(VI) sorption samples

FT-IR spectrum of the aqueous Se(VI) solution (Fig. S3b) showed only one peak at 868 cm^{-1}, corresponding to the symmetric stretching ν_3 band of tetrahedral (T_d) SeO_4^{2-} molecule (Peak and Sparks, 2002). The uncoordinated tetrahedral SeO_4^{2-} was the only species throughout our experimental pH range, as indicated by speciation calculation (Fig. S4b) (Olin et al., 2005). Similar to the Se(VI) solution, the FT-IR spectrum of solid Na_2SeO_4 had a strong band at 868 cm^{-1} (Fig. 3f). For Se(VI) sorption sample in NaCl IS (Fig. 3b), the peak at 872–875 cm^{-1} was ascribed to the shifting of the 868 cm^{-1} ν_3 band, suggesting the formation of outer-sphere complexes between Se(VI) and the composite. As indicated by previous studies (Jordan et al., 2011; Nakamoto, 2009), the formation of outer-sphere complexes did not change the symmetry of oxyanion and might only cause minor distortion and slight increase of the ν_3 mode. Such outer-sphere complexes with slightly disturbed T_d symmetry were recently observed for SeO_4^{2-} sorption on anatase (Jordan et al., 2011, 2013a).

Similarly, for Se(VI) sorption sample in $CaCl_2$ IS (Fig. 3d), the band at 872 cm^{-1} (resulted from the slight shift of the ν_3 band) also suggested the formation of outer-sphere complexes. The weak bands at 896 and 855 cm^{-1} at 3.0 M IS might indicate small contribution from inner-sphere complexes. Jordan et al. (2013b) found that, in addition to outer-sphere complexes, inner-sphere complexes also had a small (15%) contribution to Se(VI) sorption by maghemite as revealed by EXAFS. Wijnja and Schulthess (2000) also found that Se(VI) formed predominantly outer-sphere surface complexes on goethite and Al oxide at pH > 6, and inner-sphere complex only at pH < 6.

3.6. XPS analysis

XPS can provide information on the samples', elemental composition and the oxidation states of the adsorbed Se species (Han et al., 2013). The Se 3d XPS spectrum of $CaSeO_3$ (Fig. S5c) had only one strong peak with binding energy of 58.6 eV, which was ascribed to Se(IV) (Han et al., 2013). For the Ca-Se(IV) precipitate sample (Fig. S5c), the Se 3d peak shifted to higher binding energy of 59.0 eV compared to that of $CaSeO_3$, suggesting a slightly different structure from $CaSeO_3$, possibly a mixed Ca-Se(IV)/carbonate/hydroxide precipitate with different hydration states.

The Se 3d XPS spectrum of composite (Fig. S5d) could be fitted to two line shapes with binding energies at 60.3 eV and 56.0 eV, which were ascribed to the presence of minor amounts of Se(VI) in the composite (possible source from the CFA) and the interference from Fe 3p because of the presence of Fe_2O_3 in the composite (Naumkin et al., 2012), respectively. For composite that sorbed Se(IV) in NaCl medium (Fig. S5e), a strong Na 2s (63.7 eV) peak was observed, and the Se 3d peak (59.0 eV) confirmed the sorption of Se(IV) by the composite. For composite that sorbed Se(IV) in $CaCl_2$ medium (Fig. S5g), a broad peak with binding energy at 59.5 eV was observed in addition to the peak at 59.0 eV. The peak at 59.0 eV was most likely from the precipitation of Se(IV), but the composition of this precipitation needs further confirmation. The Se 3d XPS spectrum of Na_2SeO_4 showed two peaks with binding energies at 63.0 and 60.0 eV, corresponding to Na 2s and Se 3d (Fig. S5b) according to the NIST X-ray photoelectron spectroscopy database (Naumkin et al., 2012). After Se(VI) sorption to composite in NaCl or $CaCl_2$ medium, similar Se(VI) (60.0 eV) signals were observed in both spectra (Fig. S5f and h), indicating Se(VI) sorption by the composite. Previous studies also showed that the Se 3d peak of Se(VI) was located at around 59.0 eV, while the position of Se 3d peak for Se(VI) in the present study shifted to a lower binding energy (60.0–60.3 eV) compared with 61.6–62.0 eV observed in literature (Banerjee and Nesbitt, 2000; Han et al., 2013).

3.7. XRD analysis of reacted samples

The Ca-Se(IV) precipitate demonstrated different XRD patterns from the pure $CaSeO_3$ (Fig. 4 and Table S2), indicating their different structures, although they both contained Ca^{2+} and SeO_3^{2-}. This was consistent with the result of ATR-FT-IR (Fig. 3e). No known phases in the PDF database were found to match the XRD pattern of this Ca-Se(IV) precipitate. Moreover, there were several matching peaks between sorbed Se(IV)-Ca and Ca-Se(IV) precipitate, while only three matching peaks between sorbed Se(IV)-Ca, pure $CaSeO_3$, and Ca-Se(IV) precipitate. This suggested the formation of precipitate(s) for Se(IV) sorption at high IS of $CaCl_2$ (3.0 M) with a structure more similar to the Ca-Se(IV) precipitate than the pure $CaSeO_3$. The formation of $CaSeO_3 \cdot H_2O$ has also been identified when cement was utilized to immobilize Se(IV) in artificially contaminated soils (Moon et al., 2009). In addition to Ca-selenite precipitates, calcite ($CaCO_3$) precipitate was observed for sorbed Se(IV)-Na and sorbed Se(IV)-Ca, and a large amount of halite (NaCl) appeared in sorbed Se(IV)-Na.

3.8. XAS analysis of reacted samples

XAS analysis on the Ca-Se(IV) precipitate showed a local structure identical to that of $CaSeO_3$, as can be observed from both XANES and EXAFS data (Fig. 5). However, their XRD patterns (i.e. long range order) did not match with each other (Fig. 4). Since XAS is an element specific technique that is sensitive to local coordination environment (within 5–6 Å), it is possible that the Ca-Se(IV) precipitate had a different hydration state from $CaSeO_3$ or was a mixed phase with potential participation of carbonate and hydroxyl groups. A previous study on the stability of the Ca-Se(IV)-H_2O system at 25 °C determined that $Ca_2SeO_3(OH)_2 \cdot 2H_2O$ was the most stable phase at pH > 6 (Nishimura and Hata, 2007). However, the Ca-Se(IV) precipitate in our system did not match the structure of $Ca_2SeO_3(OH)_2 \cdot 2H_2O$, consistent with XRD results and suggesting its complex structure in nature.

Se(IV)-Ca and Se(IV)-Na sorption samples both can be fit with a Se-O shell with ~3 oxygen atoms at ~1.7 Å, consistent with the triangular planer structural configuration of SeO_3^{2-} (Table S4 and Fig. S6) and consistent with previous studies (e.g. Elzinga et al., 2009; Chan et al., 2009). The presence of only an oxygen shell for Se(IV)-Na sorption sample was consistent with batch and ATR-FT-IR results and suggested the predominant formation of outer-sphere complexes. These two samples also had some subtle structural difference as can be seen from XANES (Fig. 6).

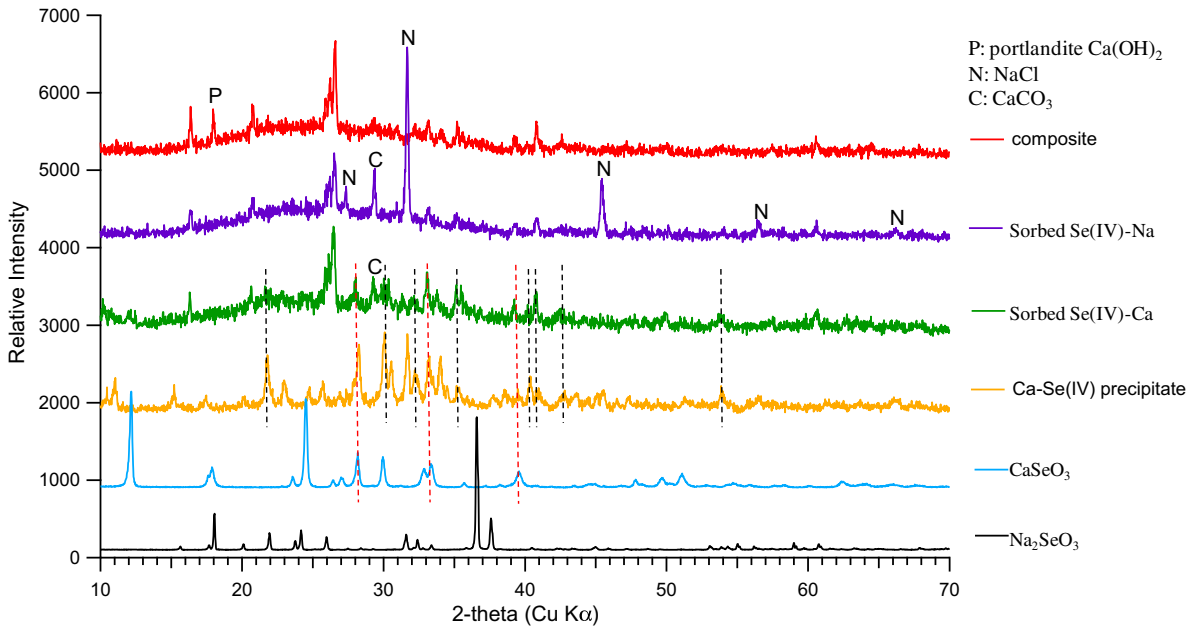

Fig. 4. XRD patterns of composite before and after Se(IV) sorption in NaCl or $CaCl_2$ background electrolyte (Sorbed Se(IV)-Na and Sorbed Se(IV)-Ca), and the Se(IV) precipitate formed in $CaCl_2 + Na_2SeO_3$ solution (Ca-Se(IV) precipitate); pure $CaSeO_3$ and Na_2SeO_3. Red dash line: the peaks present in sorbed Se(IV)-Ca, Ca-Se(IV) precipitate, and $CaSeO_3$, black dash line: the peaks present in sorbed Se(IV)-Ca and Ca-Se(IV) precipitate.

Besides the Se-O shell, the Se(IV)-Ca sorption sample also had a higher shell which could be fit with a Se-Ca path at ~3.98 Å or a Se-Se path at ~3.85 Å with similar goodness of fitting (i.e. residual) (Table S4 and Fig. S6) using $CaSeO_3$ as a structural model. The structure of $CaSeO_3$ had multiple overlapping Ca and Se shells at ~3.2–4.0 Å (i.e. 1 Ca at 3.22 Å, 1 Ca at 3.36 Å, 2 Ca at 3.49 Å, 1 Ca at 3.66 Å, 1 Ca at 3.79 Å, 1 Se at 3.80 Å, 1 Ca at 3.9 Å, 2 Se at 3.95 Å), making it very difficult to resolve each individual shells. Similar structural complexity existed for the hydrated phase $CaSeO_3 \cdot 2H_2O$. The two fitting results likely resulted from the complex local coordination environment of the Ca-selenite precipitate(s) formed during Se(IV) sorption in the presence of $CaCl_2$, and reflected the combined backscattering contributions from multiple Ca and/or Se paths at closely associated distances. In order to determine the relative contribution of precipitates in this sample, the Se(IV)-Na sorption sample (with only outer-sphere complex as suggested by ATR-FT-IR and batch sorption data) and the Ca-Se(IV) precipitate were used as end members for linear combination fitting (LCF). Good fit was obtained with 82% Se(IV)-Na sorption sample (i.e. outer-sphere) and 18% Ca-Se(IV) precipitate (Fig. S7). The 18% fraction of Ca-Se(IV) precipitate was lower than expected based on the significant changes from batch experiments, XRD, and FT-IR, possibly due to residual aqueous Se(IV) in the wet paste that contributed to the Se(IV)-Na signal. Nonetheless, the presence of Ca-Se(IV) precipitate from XAS analysis provided strong evidence and supports the analysis from other techniques.

Se(VI)-Ca and Se(VI)-Na sorption samples both can be fit with a Se-O shell with ~4 oxygen atoms at ~1.65 Å, consistent with the typical tetrahedral structural configuration of SeO_4^{2-} (Table S4 and Fig. S6) and as observed previously (e.g. Elzinga et al., 2009; Jordan et al., 2013b; Peak and Sparks, 2002). The presence of only an oxygen shell for Se(VI)-Na sorption sample was consistent with batch and ATR-FT-IR results and suggested the predominant formation of outer-sphere complexes only. For Se(VI)-Ca sorption sample, an additional Ca shell could be fitted at ~3.42 Å (Table S4 and Fig. S6), suggesting the formation of inner-sphere complex.

3.9. Sorption mechanisms

In NaCl medium, IS affected both Se(IV) and Se(VI) sorption (Fig. 1a and c), suggesting the predominant formation of outer-sphere complexes. This mechanism was confirmed by ATR-FT-IR analysis. Previous studies also showed the formation of outer-sphere complexes during Se(IV) and Se(VI) sorption to hardened cement paste and cement minerals (Bonhoure et al., 2006).

In $CaCl_2$ medium, Se(IV) showed a significant increase in sorption amount with increasing IS (0.03–3.0 M) (Fig. 1b). XRD and XAS confirmed the formation of Ca-selenite precipitates at 3.0 M $CaCl_2$. It is possible that similar precipitates or Ca-selenite-composite ternary complex were also formed at lower IS. Previous research observed a $CaSeO_3$ precipitate during Se(IV) sorption to cement minerals under high selenite concentrations (Baur and Johnson, 2003). Although we were unable to identify the exact composition or structure of the precipitates, our XRD, XPS, FT-IR, and XAS nonetheless provided strong evidences of its formation, with a structure locally similar to that of $CaSeO_3$ and possible structural and compositional contributions from carbonate or hydroxyl ions and with variable hydration states.

For Se(VI) sorption in $CaCl_2$ medium, there was a slight increase in sorption amount at lower IS (0.03–0.3 M) but no IS effect at higher IS (0.3–3.0 M) (Fig. 1d). This suggested the formation of predominantly outer-sphere complexes at all IS levels, and the additional presence of inner-sphere complexes at higher IS (>0.3 M). The strong band at 872 cm^{-1} in ATR-FT-IR spectra due to the slightly shift of the ν_3 band (Fig. 3d) supported the formation of outer-sphere complexes. Moreover, the two weak bands at 896 and 855 cm^{-1} at higher IS of 3.0 M also revealed the minor contribution from inner-sphere complexes. It was previously found that Se(VI) could form both outer-sphere and inner-sphere complexes, but the inner-sphere complexes usually exhibited much less contribution than outer-sphere complexes and/or only occur at certain experimental conditions (Jordan et al., 2013a; Wijnja and Schulthess, 2000). The effect of pH on Se(IV) and Se(VI) sorption at high IS of $CaCl_2$ (3.0 M) demonstrated the increased uptake of both Se(IV) and Se(VI) at pH > 9.5, which also highlighted the formation of precipitate for Se(IV) and presence of inner-sphere complexes for Se(VI).

3.10. Environmental implications

While PC and CFA are inexpensive or waste materials that have been widely investigated for applications in adsorbing heavy metals from

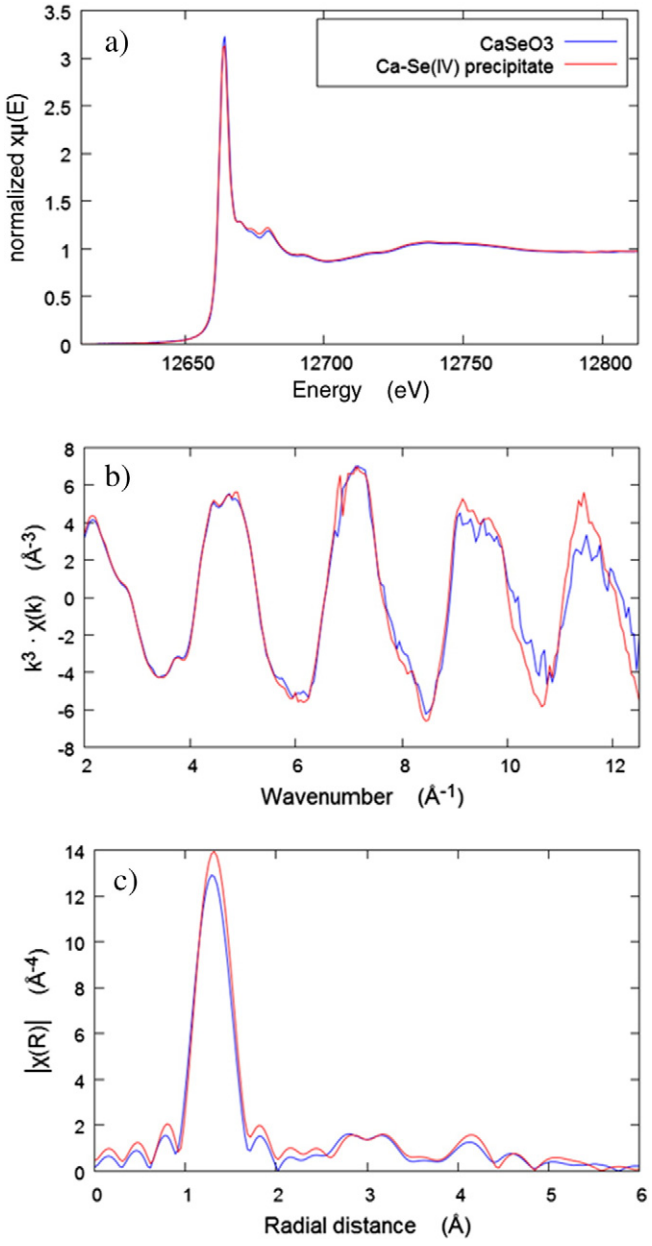

Fig. 5. Se K-edge XAS data of $CaSeO_3$ and Ca-Se(IV) precipitate, showing (a) X-ray absorption near edge structure (XANES) region, (b) k^3-weighted chi function, and (c) Fourier transforms magnitudes of the extended X-ray absorption fine structure (EXAFS) region.

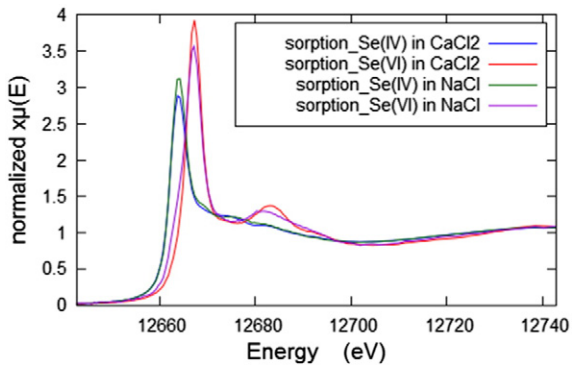

Fig. 6. Se K-edge XANES data of Se(IV) and Se(VI) sorption samples in $CaCl_2$ and NaCl background electrolytes.

wastewaters (Huang et al., 2012; Keller, 2002; Moon et al., 2009; Ochs et al., 2002), this study is among the first to investigate the immobilization of Se(IV)/Se(VI) by the CFA/PC composite under high IS condition. The results provide insight for the significant effects of cation composition (e.g. Na vs Ca) on the sorption mechanism of Se(IV) to the CFA/PC composite. For concentrated FGD brines in which Se speciation is dominated by Se(IV), a successful S/S process with CFA and PC can likely be designed with minimal chemical addition due to $CaSeO_3$ precipitation in the high Ca^{2+} and high pH conditions of the S/S process. However, the weak adsorption of Se(VI) indicated that a successful S/S for Se(VI) will require additional strategies. One possible option is to reduce Se(VI) to Se(IV) by a reductant prior to or during the S/S process. In brines in which Na^+ is the dominant cations, Se(IV) and Se(VI) are sorbed by the CFA/PC composite mostly via outer-sphere complexes; desorption and mobility of selenium remain possible in such systems due to weak adsorption. For practical implications, the high concentration of Ca^{2+} in the FGD brines will likely enhance the removal of Se(IV), but help little for Se(VI) removal. Results of this study are useful in optimizing Se removal strategies for concentrated FGD wastewater.

4. Conclusions

This study investigated the uptake behavior and mechanisms of Se(IV) and Se(VI) by a coal fly ash/cement composite at high IS of up to 3.0 M NaCl or $CaCl_2$. The IS from NaCl only caused slight increases in the uptake of Se(IV) and Se(VI), suggesting the predominant formation of outer-sphere complexes for both. In contrast, the IS from $CaCl_2$ significantly enhanced Se(IV) uptake, but had minor effect at lower IS (~0.3 M) and no effect at higher IS (>0.3 M) on Se(VI) uptake. The enhancement of Se(IV) uptake by $CaCl_2$ can be ascribed to the formation of Ca-Se(IV) precipitates. Se(VI) formed predominantly outer-sphere complexes at all IS levels, and additionally inner-sphere complexes at higher IS (>0.3 M) in $CaCl_2$ medium. The above sorption mechanisms of Se were confirmed by FTIR, XPS, XRD, and XAS.

Acknowledgements

Financial support from the China Scholarship Council (201206015012) for W. Sun is acknowledged. This study was partially supported by the Environmental Research and Education Foundation. Dr. Guangxuan Zhu (Georgia Tech) is thanked for help with ICP-OES and ATR-FT-IR analyses. We thank the beamline scientist Dr. Qing Ma at APS beamline 5-BM-D for help with experimental setup. A portion of this research was conducted at the Advanced Photon Source, a U.S. Department of Energy Office of Science User Facility operated by Argonne National Laboratory under Contract No. DE-AC02-06CH11357.

Appendix A. Supplementary data

Supplementary data to this article can be found online at http://dx.doi.org/10.1016/j.chemgeo.2016.12.041.

References

Ahrland, S., 1972. How to distinguish between inner and outer sphere complexes in aqueous solution. Thermodynamic and other criteria. Coord. Chem. Rev. 8, 21–29.
Balistrieri, L.S., Chao, T.T., 1987. Selenium adsorption by goethite. Soil Sci. Soc. Am. J. 51, 1145–1151.
Banerjee, D., Nesbitt, H.W., 2000. XPS study of reductive dissolution of birnessite by H_2SeO_3 with constraints on reaction mechanism. Am. Mineral. 85, 817–825.
Batchelor, B., 2006. Overview of waste stabilization with cement. Waste Manag. 26, 689–698.
Baur, I., Johnson, C.A., 2003. Sorption of selenite and selenate to cement minerals. Environ. Sci. Technol. 37, 3442–3447.
Bonhoure, I., Baur, I., Wieland, E., Johnson, C.A., Scheidegger, A.M., 2006. Uptake of Se(IV/VI) oxyanions by hardened cement paste and cement minerals: an X-ray absorption spectroscopy study. Cem. Concr. Res. 36, 91–98.
Boyle-Wight, E.J., Katz, L.E., Hayes, K.F., 2002a. Macroscopic studies of the effects of selenate and selenite on cobalt sorption to γ-Al_2O_3. Environ. Sci. Technol. 36, 1212–1218.

Boyle-Wight, E.J., Katz, L.E., Hayes, K.F., 2002b. Spectroscopic studies of the effects of selenate and selenite on cobalt sorption to γ-Al_2O_3. Environ. Sci. Technol. 36, 1219–1225.
Chan, Y.T., Kuan, W.H., Chen, T.Y., Wang, M.K., 2009. Adsorption mechanism of selenate and selenite on the binary oxide systems. Water Res. 43, 4412–4420.
Chappell, M.A., Seiter, J.M., Bednar, A.J., Price, C.L., Averett, D., Lafferty, B., Tappero, R., Stanley, J.S., Kennedy, A.J., Steevens, J.A., 2014. Stability of solid-phase selenium species in fly ash after prolonged submersion in a natural river system. Chemosphere 90, 174–181.
Chubar, N., 2014. EXAFS and FTIR studies of selenite and selenate sorption by alkoxide-free sol–gel generated Mg–Al–CO_3 layered double hydroxide with very labile interlayer anions. J. Mater. Chem. A 2, 15995–16007.
Conde, J.E., Sanz Alaejos, M., 1997. Selenium concentrations in natural and environmental waters. Chem. Rev. 97, 1979–2003.
Electric Power Research Institute (EPRI), 2008. Impact of Air Emissions Controls on Coal Combustion Products (1015544). Palo Alto, California.
Elrashidi, M.A., Adriano, D.C., Workman, S.M., Lindsay, W.L., 1987. Chemical equilibria of selenium in soils: a theoretical development. Soil Sci. 144, 141–152.
Elzinga, E.J., Tang, Y., McDonald, J., DeSisto, S., Reeder, R.J., 2009. Macroscopic and spectroscopic characterization of selenate, selenite, and chromate adsorption at the solid-water interface of γ-Al_2O_3. J. Colloid Interface Sci. 340, 153–159.
Essington, M.E., 1988. Estimation of the standard free energy of formation of metal arsenates, selenates, and selenites. Soil Sci. Soc. Am. J. 52, 1574–1579.
Fordyce, F., 2007. Selenium geochemistry and health. Ambio 36, 94–97.
Foster, A.L., Brown Jr., G.E., Parks, G.A., 2003. X-ray absorption fine structure study of As(V) and Se(IV) sorption complexes on hydrous Mn oxides. Geochim. Cosmochim. Acta 67, 1937–1953.
Fowless, A.D., Stranks, D.R., 1977. Selenitometal complexes. 1. Synthesis and characterization of selenito complexes of cobalt(III) and their equilibrium properties in solution. Inorg. Chem. 16, 1271–1276.
Han, D.S., Batchelor, B., Abdel-Wahab, A., 2013. XPS analysis of sorption of selenium(IV) and selenium(VI) to mackinawite (FeS). Environ. Prog. Sustain. 32, 84–93.
Hayes, K.F., Roe, A.L., Brown, G.E., Hodgson, K.O., Leckie, J.O., Parks, G.A., 1987. In situ X-ray absorption study of surface complexes: Selenium oxyanions on α-FeOOH. Science 238, 783–786.
Huang, Y.H., Peddi, P.K., Zeng, H., Tang, C., Teng, X., 2012. Pilot-scale demonstration of the hybrid zero-valent iron process for treating flue-gas-desulfurization wastewater: Part I. Water Sci. Technol. 67, 16–23.
Huang, C.-H., Burns, S., Renew, J.E., 2016. Immobilization of heavy metals by solidification/stabilization in Co-disposed coal fly ash and concentrated flue gas desulfurization wastewater brines. Environmental Research and Education Foundation Research Report, Charlotte, North Carolina.
Johnson, E.H., Rubin, M.J., Steinberg, S.M., Johnson, W.H., 2000. The sorption of selenite on various cement formulations. Waste Manag. 20, 509–516.
Jordan, N., Foerstendorf, H., Weiß, S., Heim, K., Schild, D., Brendler, V., 2011. Sorption of selenium(VI) onto anatase: macroscopic and microscopic characterization. Geochim. Cosmochim. Acta 75, 1519–1530.
Jordan, N., Müller, K., Franzen, C., Brendler, V., 2013a. Temperature impact on the sorption of selenium (VI) onto anatase. J. Colloid Interface Sci. 390, 170–175.
Jordan, N., Ritter, A., Foerstendorf, H., Scheinost, A.C., Weiß, S., Heim, K., Grenzer, J., Mücklich, A., Reuther, H., 2013b. Adsorption mechanism of selenium(VI) onto maghemite. Geochim. Cosmochim. Acta 103, 63–75.
Jordan, N., Ritter, A., Scheinost, A.C., Weiss, S., Schild, D., Hübner, R., 2014. Selenium(IV) uptake by maghemite (γ-Fe_2O_3). Environ. Sci. Technol. 48, 1665–1674.
Keller, I.R.B., 2002. The Immobilisation of Heavy Metals and Metalloids in Cement Stabilised Wastes: A Study Focusing on the Selenium Oxyanions SeO_3^{2-} and SeO_4^{2-}. Swiss Federal Institute of Technology, Zürich (doctoral dissertation).
Kretzschmar, J., Jordan, N., Brendler, E., Tsushima, S., Franzen, C., Foerstendorf, H., Stockmann, M., Heim, K., Brendler, V., 2015. Spectroscopic evidence for selenium(IV) dimerization in aqueous solution. Dalton Trans. 44, 10508–10515.
Lai, C., Yang, X., Tang, Y., Rittmann, B.E., Zhao, H., 2014. Nitrate shaped the selenate-reducing microbial community in a hydrogen-based biofilm reactor. Environ. Sci. Technol. 48, 3395–3402.
Lemly, A.D., 1993. Guidelines for evaluating selenium data from aquatic monitoring and assessment studies. Environ. Monit. Assess. 28, 83–100.
Lo, I.M., Tang, C., Li, X., Poon, C., 2000. Leaching and microstructural analysis of cement-based solidified wastes. Environ. Sci. Technol. 34, 5038–5042.
Luoma, S.N., Presser, T.S., 2009. Emerging opportunities in management of selenium contamination. Environ. Sci. Technol. 43, 8483–8487.
Manceau, A., Charlet, L., 1994. The mechanism of selenate adsorption on goethite and hydrous ferric oxide. J. Colloid Interface Sci. 168, 87–93.
Meseck, S., Cutter, G., 2012. Selenium behavior in San Francisco bay sediments. Estuar. Coasts 35, 646–657.
Moon, D.H., Grubb, D.G., Reilly, T.L., 2009. Stabilization/solidification of selenium-impacted soils using Portland cement and cement kiln dust. J. Hazard. Mater. 168, 944–951.
Nakamoto, K., 2002. Sample characterization and spectral data processing. In: Chalmers, J.M., Griffiths, P.R. (Eds.), Handbook of Vibrational Spectroscopy. Wiley.
Nakamoto, K., 2009. Infrared and Raman Spectra of Inorganic and Coordination Compounds Part B: Applications in Coordination, Organometallic, and Bioinorganic Chemistry. John Wiley & Sons.
Naumkin, A.V., Krat-Vass, A., Gaarenstroom, S.W., Powell, C.J., 2012. NIST X-ray Photoelectron Spectroscopy Database. NIST Standard Reference Database Vol. 20 (Version 4.1 (http://srdata.nist.gov/xps/)).
Nishimura, T., Hata, R., 2007. Chemistry of the Ca-Se(IV)-H_2O and Ca-Se(VI)-H_2O systems at 25 °C. Hydrometallurgy 89, 346–356.
Ochs, M., Lothenbach, B., Giffaut, E., 2002. Uptake of oxo-anions by cements through solid-solution formation: experimental evidence and modeling. Radiochim. Acta 90, 639–646.
Olin, Å., Noläng, B., Öhman, L., Osadchii, E., Rosén, E., 2005. Chemical thermodynamics of selenium. Elsevier Sci. 894.
Peak, D., 2006. Adsorption mechanisms of selenium oxyanions at the aluminum oxide/water interface. J. Colloid Interface Sci. 303, 337–345.
Peak, D., Sparks, D.L., 2002. Mechanisms of selenate adsorption on iron oxides and hydroxides. Environ. Sci. Technol. 36, 1460–1466.
Renew, J.E., Huang, C.-H., Burns, S., Carrasquillo, M., Sun, W.L., Ellison, K.M., 2016. Immobilization of heavy metals by solidification/stabilization of co-disposed flue gas desulfurization brine and coal fly ash. Energy Fuel 30, 5042–5051.
Ruhl, L., Vengosh, A., Dwyer, G.S., Hsu-Kim, H., Deonarine, A., 2010. Environmental impacts of the coal ash spill in Kingston, Tennessee: an 18-month survey. Environ. Sci. Technol. 44, 9272–9278.
Ruhl, L., Vengosh, A., Dwyer, G.S., Hsu-Kim, H., Schwartz, G., Romanski, A., Smith, S.D., 2012. The impact of coal combustion residue effluent on water resources: a North Carolina example. Environ. Sci. Technol. 46, 12226–12233.
Schwartz, G.E., Rivera, N., Lee, S.-W., Harrington, J.M., Hower, J.C., Levine, K.E., Vengosh, A., Hsu-Kim, H., 2016. Leaching potential and redox transformations of arsenic and selenium in sediment microcosms with fly ash. Appl. Geochem. 67, 177–185.
Sharmasarkar, S., Reddy, K.J., Vance, G.F., 1996. Preliminary quantification of metal selenite solubility in aqueous solutions. Chem. Geol. 132, 165–170.
Su, C., Suarez, D.L., 2000. Selenate and selenite sorption on iron oxides an infrared and electrophoretic study. Soil Sci. Soc. Am. J. 64, 101–111.
Sun, W.L., Pan, W.Y., Wang, F., Xu, N., 2015. Removal of Se(IV) and Se(VI) by MFe_2O_4 nanoparticles from aqueous solution. Chem. Eng. J. 273, 353–362.
United States Environmental Protection Agency, 2003. National Primary Drinking Water Standard. Office of Groundwater and Drinking Water (4606 M) (EPA 816-F-03-016).
United States Environmental Protection Agency, 2009. Steam Electric Power Generating Point Source Category: Final Detailed Study Report, EPA 821-R-09-08.
Wijnja, H., Schulthess, C.P., 2000. Vibrational spectroscopy study of selenate and sulfate adsorption mechanisms on Fe and Al (hydr)oxide surfaces. J. Colloid Interface Sci. 229, 286–297.
World Health Organization (WHO), 2011. Guidelines for Drinking-Water Quality. fourth ed.